

Mass-Temperature Relation of X-ray Clusters in Triaxial Halo *

Rong Yang, Jun Yu and Guo-Peng Shen

Center for Astrophysics, University of Science and Technology of China, Hefei 230026
National Astronomical Observatories, Chinese Academy of Science, Beijing 100012

Received 2003 July 10; accepted 2004 January 5

Abstract We investigate the mass-temperature relation of clusters for both the spherical NFW halo model and a concentric triaxial halo model. We study the temperature and density distributions of both an isothermal and a polytropic intra-cluster gas in hydrostatic equilibrium. We find that both the uncertainties in the concentration parameter and in the eccentricities (in case of the triaxial halo) lead to a greater scatter in the emission-weighted temperature at a given halo mass for less massive clusters. This may be helpful when determining the intrinsic statistical error of the σ_8 normalization of the linear power spectrum from cluster abundance.

Key words: cosmology: theory — galaxy: cluster: general — large-scale structure of universe

1 INTRODUCTION

As the largest virialized objects in the universe, clusters of galaxies serve as excellent cosmological indicators. In the hierarchical clustering paradigm of structure formation, the formation and evolution of clusters are sensitive to the cosmological parameters and to the amplitude of mass fluctuation. One of the strongest constraints in cosmology comes from the abundance of clusters in the local universe, which provides a direct handle on the matter power spectrum on scales of a few megaparsec and hence a normalization scheme for the linear power spectrum (White, Efstathiou & Frenk 1993; Bond & Myers 1996; Viana & Liddle 1996; Kitayama & Suto 1997; Eke et al. 1998; Pen 1998; Wang & Steinhardt 1998; Blanchard et al. 2000; Henry 2000; Pierpaoli, Scott & White 2001; Borgani et al. 2001; Seljak 2001). Moreover, the cluster population at higher redshifts is sensitive to the linear growth rate of density fluctuations, which allows us to break the Ω_M - σ_8 degeneracy from the local abundance constraints (Eke, Cole & Frenk 1996; Bahcall & Fan 1998).

Underlying the σ_8 normalization is the Press-Schechter formulation for the evolution of the number density of dark matter halos originated from the initial Gauss fluctuations. The theory works with the virial cluster mass, which is difficult to measure observationally, so a more promising technique is to convert the virial mass to the observable X-ray temperature. So far, there has been a great effort to set up the mass-temperature relation from some semi-analytical model or hydrodynamic simulation (Bryan & Norman 1998; Horner et al. 1999; Voit 2000;

* Supported by the National Natural Science Foundation of China.

Afshordi & Cen 2002). The simple virialization model suggests the mass scaling to the power $3/2$ of the temperature, $M \propto T^{3/2}$. It is noted that both simulations and observations reproduce the predicted slope of M - T relation, while yielding a wide range for the proportionality coefficient. Uncertainties may arise from complex modeling of physical processes in the simulation, insufficient resolution, and various working definitions of temperature in the observations. Clearly, only a reliable normalization of the M - T relation with a well quantified scatter allows precise measurement of the cosmological fluctuation power spectrum.

The key issue in understanding the M - T relation is the distribution of the X-ray emitting intra-cluster gas. The current, widely-used simple description for the gas is the spherical isothermal β model. The more remarkable progress was the recognition of a universal scaling behavior of the density profile in simulated halos by Navarro, Frenk & White (1996, 1997, hereafter NFW). The hydrostatic equilibrium solution of the intra-cluster gas embedded in the spherical NFW model and its application to X-ray clusters have been also investigated (Makino, Sasaki & Suto 1998; Suto, Sasaki & Makino 1998; Komatsu & Seljak 2001).

Obviously, a direct generalization of dark matter halos beyond the spherical model is the aspherical model, whose importance has been realized in understanding some observed properties, including X-ray morphologies of clusters (Buote et al. 2002) from Chandra observations, and the Hubble constant measurement via the Sunyaev-Zeldovich effect (Birkinshaw, Hughes & Arnaud 1991; Inagaki, Sugimotohara & Suto 1995; Yoshikawa, Itoh & Suto 1998). By means of N-body simulation with high resolution, Jing & Suto (2002, hereafter JS02) demonstrated a more realistic model with a triaxial halo density profile. Because of their cosmological importance, the probability distributions of the axis ratio and the concentration parameter were quantified by a set of fitting formulae. Subsequently, an analytical approach to the intra-cluster gas in the triaxial model and application to arc statistics have been presented (Lee & Suto 2003; Oguri, Lee & Suto 2003).

The primary interest of this paper is to investigate the M - T relation statistically in the triaxial halo model, in particular, the intrinsic scatter in the M - T relation arising from random statistical distribution of the halo shapes. The paper is organized as follow, Sect. 2 gives a brief sketch of both the spherical and triaxial modeling of dark matter halo. The density and temperature of intra-cluster gas distribution in hydrostatic equilibrium are numerically solved. Then, in Sect. 3 we study statistically the M - T relation by a Monte-Carlo sample of triaxial clusters, and discuss the effect of asphericity on the normalization of the M - T relation. Sect. 4 presents our concluding remarks.

2 TRIAXIAL MODELING OF DARK MATTER HALOS

2.1 The NFW Spherical Model

Based on high resolution N-body simulation, the dark matter density profile was suggested to follow a universal form by NFW,

$$\frac{\rho_{\text{DM}}(r)}{\rho_{\text{crit}}} = \frac{\delta_c}{(r/r_s)(1+r/r_s)^2}, \quad (1)$$

where ρ_{crit} is the critical density of the universe; the characteristic halo density contrast δ_c and the scaling radius r_s can be written in terms of the concentration parameter c_{vir} as

$$\delta_c = \frac{\Delta_{\text{vir}}}{3} \frac{c_{\text{vir}}^3}{\ln(1+c_{\text{vir}}) - c_{\text{vir}}/(1+c_{\text{vir}})}, \quad (2)$$

$$r_s(M) = \frac{r_{\text{vir}}(M)}{c_{\text{vir}}}, \quad (3)$$

in which $r_{\text{vir}} = r_{\text{vir}}(M, z)$ is the virial radius calculated by the spherical collapse model (Peebles 1970)

$$r_{\text{vir}} = \left(\frac{3M}{4\pi\Delta_{\text{vir}}\Omega_0\rho_{\text{crit}}} \right)^{\frac{1}{3}}, \quad (4)$$

in which we use Δ_{vir} within r_{vir} instead of spherical overdensity of 200 within r_{200} given by NFW. In the flat models, we adopt the fitting formula of Bryan & Norman (1998),

$$\Delta_{\text{vir}}(z) = 18\pi^2 + 82(\Omega(z) - 1) - 39(\Omega(z) - 1)^2. \quad (5)$$

For the concentration parameter c_{vir} , there have been several different fitting formulae proposed so far. In this paper, we use the formula of Bullock et al. (2001),

$$c_{\text{vir}} = \frac{9}{1+z} \left(\frac{M}{1.5 \times 10^{13} h^{-1} M_{\odot}} \right)^{-0.13}. \quad (6)$$

It is noted that there is a large scatter in c_{vir} values for a given fixed mass. The simulations suggested that c_{vir} follows a log-normal distribution:

$$p(c_{\text{vir}})d(c_{\text{vir}}) = \frac{1}{\sqrt{2\pi}\sigma_{c_{\text{vir}}}} \exp \left[-\frac{(\ln c_{\text{vir}} - \ln \bar{c}_{\text{vir}})^2}{2\sigma_{c_{\text{vir}}}^2} \right] d \ln c_{\text{vir}} \quad (7)$$

with $\sigma_{c_{\text{vir}}} \approx 0.2$. As will be discussed later, the wide spread in c_{vir} may lead to some uncertainties in the distribution of the intra-cluster gas and hence scatter in the M - T relation. Clearly, for a dark matter halo of a given virial mass M_{vir} and a sampling value of c_{vir} from the log-normal distribution, its density profile is uniquely specified.

2.2 The Triaxial Halo Model

The density profiles of triaxial halos are well approximated by a sequence of concentric and aligned triaxial distributions (Jing & Suto 2002). Similar to the NFW model, it takes the form parameterized by

$$\frac{\rho(R)}{\rho_{\text{crit}}} = \frac{\delta_c}{(R/R_0)^\alpha (1 + R/R_0)^{3-\alpha}}, \quad (8)$$

where

$$R^2 = c^2 \left(\frac{x^2}{a^2} + \frac{y^2}{b^2} + \frac{z^2}{c^2} \right),$$

a , b , and c are the three axial lengths. Without loss of generality, it is assumed that $a \leq b \leq c$. The inner slope α is not precisely quantified from the N-body simulation, it spans a range between 1 and 1.5 (Navarro et al. 1996,1997; Moore et al. 1999; Jing & Suto 2000). In this paper, we adopt the value $\alpha = 1$.

The characteristic halo density contrast δ_c , and the scaling radius R_0 in the triaxial model are also written in terms of the concentration parameter c_e

$$\delta_c = \frac{\Delta_e}{3} \frac{c_e^3}{\ln(1+c_e) - c_e/(1+c_e)}, \quad (9)$$

$$R_0 = \frac{R_e}{c_e}, \quad (10)$$

where R_e is defined such that the mean density within the ellipsoid of major axis radius R_e is $\Delta_e \rho_{\text{crit}}$

$$\Delta_e = 5\Delta_{\text{vir}} \left(\frac{c^2}{ab} \right)^{0.75}. \quad (11)$$

This unusual definition is chosen so as to have R_e a fixed fraction of the virial radius r_{vir} in the corresponding spherical NFW model for a given halo mass, i.e., Eq. (4). According to JS02, $\eta \equiv R_e/r_{\text{vir}} \approx 0.45$. Formally, we may also introduce the virial radius R_{vir} in the triaxial model, which is obtained by the equalization of mass within the ellipsoid of major axis radius R_{vir} with a pre-defined mass M_{vir} . Thus, we have

$$M_{\text{vir}} = 4\pi R_0^3 \delta_c \rho_{\text{crit}} \left(\frac{ab}{c^2} \right) g(R_{\text{vir}}/R_0), \quad (12)$$

where $g(x)$ is defined by $g(x) = \ln(1+x) - \frac{x}{1+x}$. Given the above procedures, once the shape of the ellipsoid is specified, we are able to determine the density profile for the individual triaxial halo.

In order to study the M - T relation statistically, the probability distribution function (PDF) of the shapes of halos is required. We adopt the PDFs given by JS2002, drawn from their high resolution N-body simulation in the LCDM model, which assumed $\Omega_0 = 0.3$, $\lambda_0 = 0.7$, $\sigma_8 = 0.9$ and $\Gamma = 0.2$. According to empirical formulae in JS02, introduce the scaling of the axis ratio a/c

$$\tilde{r}_{ac} = \left(\frac{a}{c} \right) \left(\frac{M_{\text{vir}}}{M_\star} \right)^{0.07[\Omega(z)]^{0.7}}, \quad (13)$$

where M_\star is the characteristic nonlinear mass at redshift z such that the rms top-hat filtered overdensity at this scale $\sigma(M_\star, z)$ is $\delta_c = 1.68$, the PDF of axis ratio is thus given by a universal form independent of the halo mass

$$p(\tilde{r}_{ac}) d\tilde{r}_{ac} = \frac{1}{\sqrt{2\pi}\sigma_s} \exp \left[-\frac{(\tilde{r}_{ac} - 0.54)^2}{2\sigma_s^2} \right] d\tilde{r}_{ac} \quad (14)$$

with $\sigma_s = 0.113$. Accordingly, the conditional probability of a/b for a given value of a/c is

$$p(a/b|a/c) = \frac{3}{2(1-r_{\text{min}})} \left[1 - \left(\frac{2a/b - 1 - r_{\text{min}}}{1 - r_{\text{min}}} \right)^2 \right] \quad (15)$$

for $a/b > r_{\text{min}}$, where $r_{\text{min}} = a/c$ for $a/c \geq 0.5$, $r_{\text{min}} = 0.5$ for $a/c < 0.5$, and $p(a/b|a/c) = 0$ for $a/b \leq r_{\text{min}}$. As in the case of the spherical NFW model, the concentration parameter c_e here also has a large scatter. The PDF for c_e is found to be well fitted by the log-normal distribution with mean value,

$$c_e[\tilde{r}_{ac}, M, z] = 1.35 A_e \sqrt{\frac{\Omega(z)\Delta_{\text{vir}}(z_c)}{\Omega(z_c)\Delta_{\text{vir}}(z)}} \left(\frac{1+z_c}{1+z} \right)^{3/2} \exp \left[-\left(\frac{0.3}{\tilde{r}_{ac}} \right)^2 \right], \quad (16)$$

and a dispersion $\sigma_{c_e} = 0.3$, where z_c is the collapse redshift of the halo of mass M , $A_e = 1.1$ for the LCDM model.

3 INTRA-CLUSTER GAS DISTRIBUTION IN DARK MATTER HALOS

For modeling the intra-cluster gas distribution in a dark matter halo, we assume that the gas is in hydrostatic equilibrium in the gravitational field generated by the halo and that the self-gravity of the baryonic gas is neglected. The equation of state of the intra-cluster gas is taken to be either isothermal or polytropic.

3.1 Gravitational Potential of Dark Matter Halos

In the spherical halo model, the gravitational potential is given by

$$\Phi(r) = - \int_r^\infty \frac{GM(r)}{r^2} dr. \quad (17)$$

For the NFW density profile, the mass enclosed within radius r is

$$M(r) = 4\pi r_s^3 \delta_c \rho_{\text{crit}} g(r/r_s), \quad (18)$$

and the gravitational potential is then given by the following expression:

$$\Phi(r) = - \frac{\ln(1 + r/r_s)}{g(r_{\text{vir}}/r_s)} \frac{r_{\text{vir}}}{r} \left[\frac{GM_{\text{vir}}}{r_{\text{vir}}} \right]. \quad (19)$$

The gravitational potential due to the ellipsoidal bodies can be written as (Binney & Tremaine 1987),

$$\Phi(\mathbf{r}) = -\pi G \left(\frac{ab}{c} \right) \int_0^\infty \frac{[\psi(\infty) - \psi(m)]}{\sqrt{(\tau + a^2)(\tau + b^2)(\tau + c^2)}}, \quad (20)$$

with

$$\psi(m) = 2 \int_0^m \rho(R) R dR, \quad (21)$$

$$m = c \sqrt{\frac{x^2}{\tau + a^2} + \frac{y^2}{\tau + b^2} + \frac{z^2}{\tau + c^2}}, \quad (22)$$

where τ labels the isopotential triaxial surfaces, on which $m = m(\mathbf{r}, \tau)$ is a constant. For the triaxial halo density profile described in Sect. 2.2, simple algebra yields

$$\Phi(\mathbf{r}) = -5\alpha \left(\frac{ab}{c^2} \right)^{1/4} \frac{c_e}{g(c_e)} G(e_a, e_b, \mathbf{r}) \left[\frac{GM_{\text{vir}}}{r_{\text{vir}}} \right], \quad (23)$$

where

$$G(e_a, e_b, \mathbf{r}) = \int_0^1 \frac{d\mu}{\sqrt{(1 - e_a^2 \mu^2)(1 - e_b^2 \mu^2)}} \frac{1}{1 + \frac{\mu}{R_0} \sqrt{\frac{x^2}{1 - e_a^2 \mu^2} + \frac{y^2}{1 - e_b^2 \mu^2} + z^2}}, \quad (24)$$

$\alpha \equiv R_e/r_{\text{vir}}$ takes the value 0.45 approximately, and the eccentricities are

$$e_a = \sqrt{1 - \frac{a^2}{c^2}} \geq e_b = \sqrt{1 - \frac{b^2}{c^2}}. \quad (25)$$

The values of e_σ^2 ($\sigma = b, c$) measure the deviations of the ellipsoidal iso-density from the spherical along the two specified directions. In general, the potential can only be obtained by numerical integration.

3.2 Temperature Distribution of Intra-cluster Gas

3.2.1 Isothermal Gas

Here we adopt the virial temperature as the temperature of the cluster. According to the virial theorem,

$$E_f + K_f = 0, \quad (26)$$

where E_f is the total energy of a virialized cluster; K_f is its kinetic energy given by

$$K_f = \frac{3}{2}M_{\text{DM}}\sigma_v^2 + \frac{3M_{\text{gas}}k_B T}{2\mu m_p}, \quad (27)$$

where σ_v is the mass-weighted mean one-dimensional velocity dispersion of dark matter particles, M_{DM} the total dark matter mass, k_B the Boltzmann constant, $\mu = 0.59$ the mean molecular weight and m_p the proton mass. Usually, it is assumed that $M_{\text{gas}}/M_{\text{DM}} = \Omega_b/\Omega_m$, $f = M_{\text{baryon}}/M_{\text{gas}}$. Hydrodynamic simulations show that only a small fraction of the baryons contribute to galaxy formation in large clusters (e.g., Blanton et al. 2000) and so f is close to one. Then we have

$$K_f = \frac{3\beta_{\text{spec}}MkT}{2\mu m_p} \left[1 + (f\beta_{\text{spec}}^{-1} - 1)\frac{\Omega_b}{\Omega_m} \right], \quad (28)$$

with $\beta_{\text{spec}} = \sigma_v^2/(kT/\mu m_p)$. The hydrodynamic simulations imply $\beta_{\text{spec}} \sim 1$.

So, the virial temperature of clusters is

$$kT = -\frac{\mu m_p U_f}{3\beta_{\text{spec}}M \left[1 + (f\beta_{\text{spec}}^{-1} - 1)\frac{\Omega_b}{\Omega_m} \right]}, \quad (29)$$

where U_f is the final potential energy,

$$U_f = \frac{1}{2} \int \rho \Phi dV. \quad (30)$$

3.2.2 Polytropic Gas

The polytropic state of the ideal gas is expressed by

$$P_g(\mathbf{r}) = P_0[\rho_g(\mathbf{r})/\rho_0]^\gamma, \quad (31)$$

where $\gamma \neq 1$ is the polytropic index. Under the assumption of hydrostatic equilibrium, the density and temperature distributions are found to be

$$T(\mathbf{r}) - T(0) = \frac{\gamma - 1}{\gamma} \frac{\mu m_p}{\kappa_B} (\Phi(0) - \Phi(\mathbf{r})), \quad (32)$$

$$\frac{\rho_g(\mathbf{r})}{\rho_0} = \left[1 - \frac{\gamma - 1}{\gamma} \frac{\mu m_p}{\kappa_B T_0} (\Phi(\mathbf{r}) - \Phi(0)) \right]^{\frac{1}{\gamma-1}}, \quad (33)$$

where T_0 is the temperature at the cluster center. Following Komatsu & Seljak (2001), we further assume that the gas density profile traces the dark matter density profile in the outer region of both triaxial and spherical halos. that is,

$$\nabla \ln \rho_g(\mathbf{r}) = \nabla \ln \rho_{\text{dm}}(\mathbf{r}). \quad (34)$$

Actually, the gas density profiles of triaxial halos derived from hydrostatic equilibrium are concentric ellipsoids of different ellipses; however, since the simulations have observed that the regions outside the core $r \gtrsim r_{\text{vir}}/2$ (Navarro, Frenk & White 1995; Bryan & Norman 1998; Eke, Navarro & Frenk 1998; Frenk et al. 1999; Pearce et al. 2000; Lewis et al. 2000; Yoshikawa, Jing & Suto 2000) were traced with 10% or better accuracy, we can use Eq. (34) to determine approximately T_0 and γ of a given halo .

For spherical halos, following

$$\rho_g^{-1} \frac{dP_g}{dr} = -G \frac{M}{r^2} \quad (35)$$

from Eq. (31) and scaling the gas density profile by $y_g(r/r_s) = \rho_g(r)/\rho_g(0)$, we obtain

$$\frac{dy_g^{\gamma-1}(r/r_s)}{dr} = -\left(\frac{\gamma-1}{\gamma}\right) \frac{G\mu m_p M_{\text{vir}}}{k_B T(0) r^2} \left[\frac{g(r/r_s)}{g(c)} \right]. \quad (36)$$

Moreover, define the normalization factor $\eta(x) \equiv 3r_{\text{vir}} k_B T_g(x)/G\mu m_p M_{\text{vir}}$ and let s_* denote an effective slope of the dark matter density profile at x_* , where the gas density profile $y_g(x)$ and the dark matter density profile $y_{\text{dm}}(x) \equiv \rho_{\text{dm}}(r)/\rho_0$ follow each other as mentioned above, Eq. (34) can be rewritten as

$$s_* \equiv \left. \frac{d \ln y_{\text{dm}}(x)}{d \ln x} \right|_{x=x_*} = \left. \frac{d \ln y_g(x)}{d \ln x} \right|_{x=x_*}. \quad (37)$$

Accordingly, T_0 is related to γ by

$$\eta(0) = \gamma^{-1} \left\{ \left(\frac{-3}{s_*} \right) \left[\frac{x_*^{-1} g(x_*)}{c_{\text{vir}}^{-1} g(c_{\text{vir}})} \right] + 3(\gamma-1) \left[\frac{c_{\text{vir}}}{g(c_{\text{vir}})} \right] \left[1 - \frac{\ln(1+x)}{x} \right] \right\}, \quad (38)$$

where $\eta(0) \equiv 3r_{\text{vir}} k_B T(0)/G\mu m_p M_{\text{vir}}$ and $s_* \equiv -[1 + 2x_*/(1+x_*)]$. In order to make $\eta(0)$ constant with different x_* where the two profiles follow each other, we vary γ from 1.0 to 1.4 to find the value at which $\eta(0)$ has the minimal rms with x_* ranging from $c_{\text{vir}}/2$ to $2c_{\text{vir}}$. Figure 1 shows that the results are similar to the simple linear fit $\gamma = 1.15 + 0.01(c_{\text{vir}} - 6.5)$ given by Komatsu & Seljak (2001), thus the polytropic index γ can be fixed with which $T(0)$ and hence $T(\mathbf{r})$ can be calculated.

In the case of triaxial halo, using the match assumption Eq. (34) and the density distribution of Eqs. (33) and (8), we obtain

$$\left(\frac{1}{R} + \frac{2}{R+R_0} \right) \nabla R = \frac{3}{\gamma} \psi_g \eta^{-1}(0) \left[\nabla G(\mathbf{r}) + (\gamma-1)(G(\mathbf{r}) - G(0)) \left(\frac{1}{R} + \frac{2}{R+R_0} \right) \nabla R \right], \quad (39)$$

where $\psi_g = -5\alpha \frac{ab^{1/4}}{c^2} \frac{c_e}{g(c_e)}$ and $G(\mathbf{r})$ defined in Eq. (24). As mentioned before, the gas density profiles in a triaxial halo are concentric ellipsoids with different ellipses. Thus, Eq. (39) has no exact solution. However, for a given triaxial halo, we can always find a γ such that $\eta(0)$ is constant for $R \in [1/2R_{\text{vir}}, 2R_{\text{vir}}]$ for each of the axes. This behavior is illustrated in Fig. 2.

Finally, we average γ and $\eta(0)$ over the three axes. While there is a simple linear fit for spherical halos given by Komatsu & Seljak (2001), with mass ranging from $10^{13} M_\odot$ to $10^{15} M_\odot$, it is hard to find a fitting formula for the triaxial halo, but for a halo of a given shape and concentration, we can use Eq. (39) to fix γ and $\eta(0)$, and hence derive $T(\mathbf{r})$ from the $T(0)$ - $\eta(0)$ relation.

The above equations give the density and temperature distributions of the intra-cluster gas within a dark matter halo. The gas temperature cannot be measured directly in X-ray observation, instead, the emission weighted temperature is often used. The X-ray emission-weighted mean temperature T_X is defined by

$$T_X = \frac{\int dV \rho_g^2 \alpha_x(T_g) T_g}{\int dV \rho_g^2 \alpha(T_g)}, \quad (40)$$

where α_x is the X-ray emissivity. For the bolometric bremsstrahlung emission, $\alpha(T_g) \propto T_g^{1/2}$. Obviously, the gas temperature and emission-weighted mean temperature are the same for isothermal halos, but in general, the two differ in the temperature gradient. In what follows, we will use T_X in the discussion of the normalization of the mass-temperature relation.

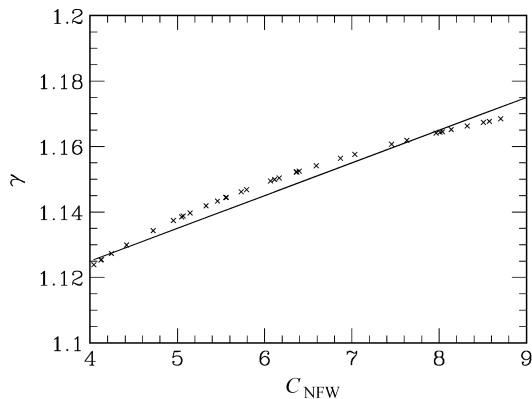


Fig. 1 We fit γ by minimizing the rms of $\eta(0)$ as x_* ranges from $c_{\text{vir}}/2$ to $2c_{\text{vir}}$. The points are close to the linear fitting formula $\gamma = 1.15 + 0.01(c_{\text{vir}} - 6.5)$ given by Komatsu & Seljak (2001).

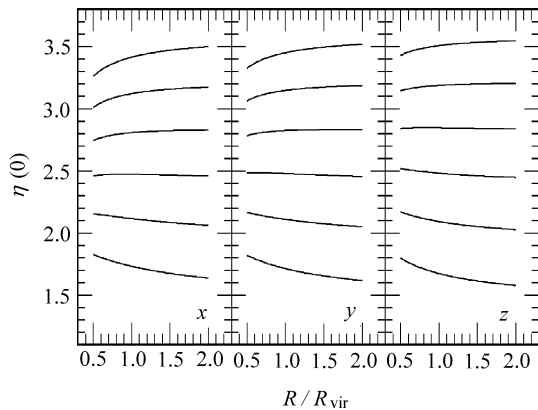


Fig. 2 Predicted $\eta(0)$ for different γ ($\gamma = 1.10, 1.14, 1.18, 1.22, 1.26, 1.30$ from bottom up in each panel), separately for each axis. Mass of the halo, $10^{14} M_{\odot}$.

4 THE MASS-TEMPERATURE RELATION IN HALO MODELS

As discussed in Sect. 2, the density profile of a dark matter halo is not uniquely specified by its mass, and there could be quite a difference between halos of the same mass. In the spherical NFW model, the long-tailed behavior of the log-normal distribution of the concentration parameter may lead to a wide range of core sizes, which will alter the density profile on the small scales. Moreover, in triaxial models, additional uncertainties come from the different shapes of ellipsoids, as described in Sect. 2.2. This section is to make a statistical investigation of the mass-temperature relation taking into account of the statistical distributions of both the concentration parameters and the eccentricities of dark matter halos.

We make a cluster sample with masses ranging from $10^{12} - 10^{16} M_{\odot}$ using Monte-Carlo method. For a given mass, we generate a sub-sample of 500 clusters each with a random sampling according to the PDFs of the concentration parameter and the axis ratio. The gravitational potential for each cluster is then calculated for the given density profile and hence the temperature of the intra-cluster gas is estimated for both the isothermal and polytropic cases, and the scatter in the $M-T$ relation is then obtained.

4.1 Mass-Temperature Relation in Isothermal Gas Model

In the isothermal model of intra-cluster gas, we use the virial theorem to estimate the X-ray temperature using Eq. (29). Figures 3 and 4 display the $M-T$ relations obtained for the spherical and triaxial halo, respectively. Clearly, for the spherical halo, the spread in the virial temperature decreases with increasing mass. In contrast, the triaxial halo shows the opposite behavior, the scatter in temperature increases with increasing mass. In the former,

the only source of the scatter in the M - T relation is the random distribution of the concentration parameter c_s . Since the mean value of c_s is a decreasing function of the mass, its effect on the M - T relation is easily understood. In contrast, for the triaxial halo, the more massive clusters could have proportionately larger differences in their shapes, which more than compensate the effect of the concentration parameter and dominate the behaviour of the scatter.

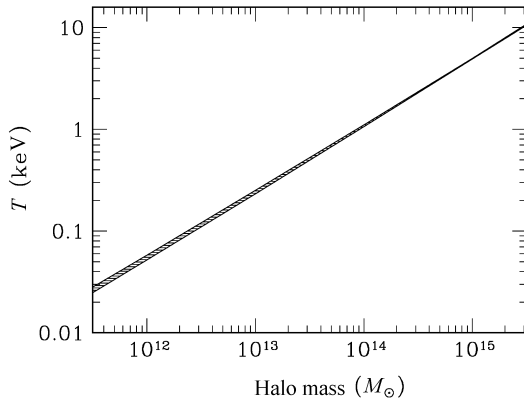


Fig. 3 Mass-temperature relation for the spherical halo model where the intra-cluster gas is assumed to be isothermal. The shaded area marks the 80% confidence interval of the temperature.

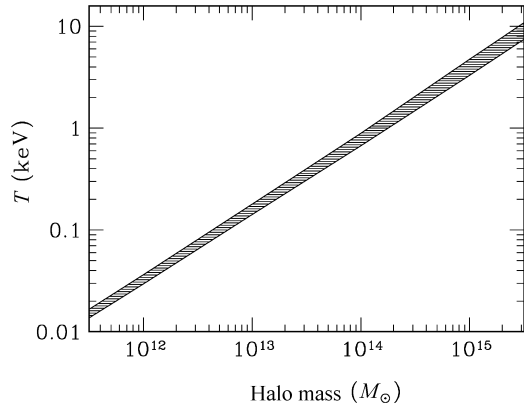


Fig. 4 Mass-temperature relation for the triaxial halo model where the intra-cluster gas is assumed to be isothermal. The shaded area marks the 80% confidence interval of the temperature.

We applied the least squares fitting to obtain the M - T relation for the Monte-Carlo samples. It is found that the samples are well fitted by the following relation,

$$T = (1.369_{-0.012}^{+0.050}) \left(\frac{M}{10^{14} h^{-1} M_{\odot}} \right)^{0.653_{-0.008}^{+0.005}} \quad (41)$$

for the spherical NFW model, and

$$T = (0.944_{-0.074}^{+0.235}) \left(\frac{M}{10^{14} h^{-1} M_{\odot}} \right)^{0.681_{-0.003}^{+0.016}} \quad (42)$$

for the triaxial model. As the PDF of temperature at a given mass does not follow a Gaussian distribution, the mean value in these relations were given by the most likely value inferred from the PDF of temperature, while the errors are given by the upper and lower bounds of the 80% confidence range.

It is obvious that the mass-virial temperature relation in the NFW model is similar to that deduced from the simple virial theory, i.e, $M \sim T^{1.5}$. The M - T relation in the triaxial model is approximately, $M \sim T^{1.47}$, however, with a lower slope. If we apply a low-pass filter and remove all clusters with virial temperatures < 3.5 keV, then the M - T relation will be close to $M \sim T^{1.5}$. This temperature of 3.5 keV is possibly a limit to judge whether it is dominated by the gravitational potential (Mohr & Evrard 1997; Balogh et al. 1999; Xue & Wu 2000).

It is not difficult to reproduce the observational slope of the M - T relation from either analytical models or hydrodynamic simulations. However, the proportionality coefficient in the M - T relation is not self-consistently determined. As given by Eqs. (41) and (42), there exists an average 25% intrinsic variance in the normalization of M - T relation. Compared to the primary

M - T relations compiled by Horner et al. (1999), we note that the proportionality coefficients in both spherical and triaxial models are higher. The reason is partially due to the working definition of X-ray temperature. In this subsection, the discussion is given for the simplified isothermal model. In the following subsection, we will consider the more realistic polytropic model of the intra-cluster gas.

4.2 Mass-Temperature Relation in Polytropic Gas Model

The density and temperature distributions of a polytropic intra-cluster gas are computed using Eqs. (32) and (33), and with Eqs. (23) and (24) for the gravitational potential for triaxial halos. To match the X-ray observations, the emission-weighted mean temperatures are used as defined by Eq. (40).

For a given mass, scatter in the temperature arises from the scatter in the concentration parameter and, for the triaxial models, also from the scatter in the eccentricities. To study their separate effects on the distribution of temperature, we fix the concentration parameter at its median value \bar{c}_e so as to isolate the eccentricity effect. The distributions of emission-weighted temperature for different halo masses are given by the histograms in Fig. 5. Clearly, it shows a significant difference between low and high halo masses. In the case of low halo mass, e.g., $10^{12-13} M_\odot$, the PDF of temperature extends downward while having a cutoff at the high temperature end. The spread becomes narrower with increasing halo mass. For $10^{15-16} M_\odot$ halo mass, the PDF shows also has a cutoff at the low temperature end. When we allow both the concentration parameter and the halo shapes to vary, then we obtain the results displayed in Fig. 6. Recall that the concentration parameter has a larger scatter at low mass than at high mass, it is easy to understand that the long-tail feature in Fig. 6, where the effect of the concentration parameter is added to the effect of the eccentricities alone shown in Fig. 5.

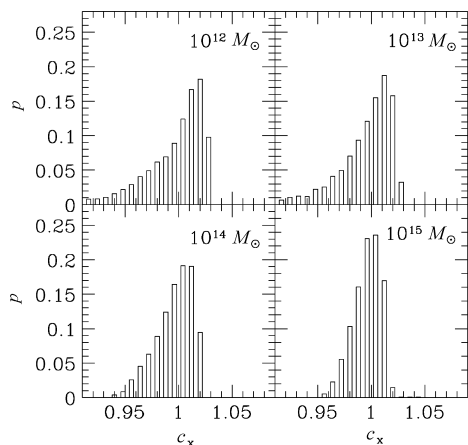


Fig. 5 Probability distribution of emission weighted temperature at a fixed value of the concentration parameter. The horizontal axis is $c_x = T/T_{\text{average}}$, the vertical axis is its probability distribution.

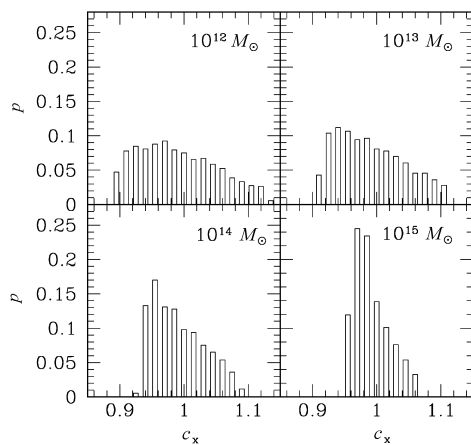


Fig. 6 Probability distribution of the emission weighted temperature, when the spread is taken into account in both the concentration parameter and the halo eccentricities.

The M - T relations found in the Monte-Carlo samples are plotted in Fig. 7 for the spherical NFW halo and in Fig. 8 for the triaxial halo, in which the intra-cluster gas is polytropic. Obviously, the results are similar to what we have found in the case where the gas is isothermal. However, for the spherical halo, the scatter in temperature is larger in the polytropic than in the isothermal case. For the triaxial halo, it is the other way round, the scatter is somewhat smaller in the polytropic than the isothermal case. It is noticed that in the NFW spherical model the fluctuation of potential at a fixed cluster mass arises from the spread in the concentration parameter, which specifies the high density region around the center of the cluster; while in the case of the triaxial halo model, it is the shape distribution that mostly leads to the potential scatter at the outer parts of the cluster. Since the emission-weighted temperature Eq. (35) is measured by the density weight $\rho_g^{(\gamma+3)/2}$, it is contributed mainly by the gas within the core of the cluster and is therefore less sensitive to the shape of cluster. Consequently, the mass-virial temperature relation has a larger scatter than the mass-emission weighted temperature relation for the triaxial halo and a smaller scatter for the spherical halo.

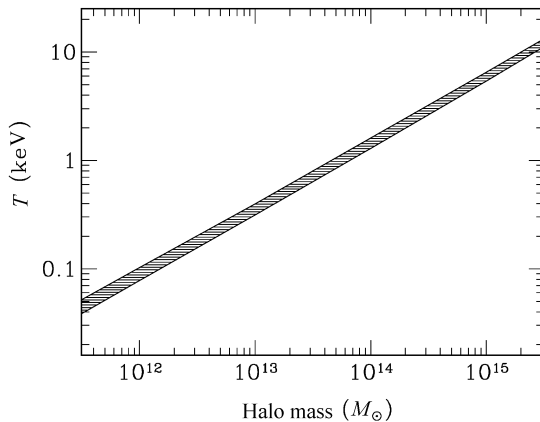


Fig. 7 Mass-temperature relation in the spherical halo model with a polytropic intra-cluster gas. The shaded area marks the 80% confidence range for the temperature.

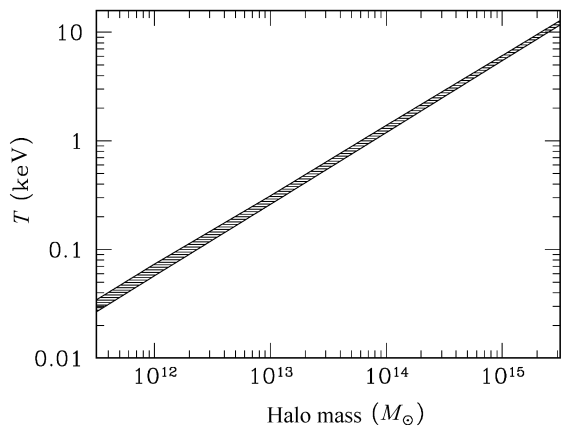


Fig. 8 Mass-temperature relation in the triaxial halo model with a polytropic intra-cluster gas. The shaded area marks the 80% confidence range of the temperature.

A least squares fitting gives the M - T relation for the spherical NFW halo (polytropic gas) as

$$T = (1.759^{+0.237}_{-0.145}) \left(\frac{M}{10^{14} h^{-1} M_{\odot}} \right)^{0.599^{+0.123}_{-0.001}}, \quad (43)$$

and for the triaxial halo (polytropic gas),

$$T = (1.553^{+0.042}_{-0.197}) \left(\frac{M}{10^{14} h^{-1} M_{\odot}} \right)^{0.643^{+0.005}_{-0.047}}. \quad (44)$$

The mean values and errors have the same meaning as those we have defined in the case of the isothermal gas.

The deduced mass-polytropic temperature relation in the NFW model is ($M \sim T^{1.67}$), its slope is higher than the result given by the simple virial theory ($M \sim T^{1.5}$). In the triaxial

model the deduced M - T relation has a slope close to the result given by the simple virial theory, but a higher coefficient than the result obtained by EMN (Evrard et al. 1996).

5 CONCLUSIONS

In the context of the NFW model and the triaxial model, we studied the density and temperature distributions of the intra-cluster gas, which is assumed to be either isothermal or polytropic gas in hydrostatic equilibrium embedded in a dark matter halo. Furthermore, adopting the statistical distributions of the concentration parameter and eccentricities of halos inferred from the N-body simulations, we present a Monte Carlo investigation of the scatter in the mass-temperature relation of galaxy clusters.

It is worth noting that uncertainty in the concentration parameter of the cluster is an important source of the scatter in the M - T relation. If the concentration parameter for a given mass cluster obeys the log-normal distribution, it will lead to an asymmetric PDF of X-ray gas temperature with a long tail. Since the mean value of the concentration parameter is a decreasing function of the cluster virial mass, the scatter in the temperature increases with decreasing cluster mass.

However, in the triaxial model, the scatter in the derived mass-temperature relation is sensitive to both the uncertainty of the concentration parameter and in the shape distribution. While the former has more effect on the core of the cluster, the latter mostly leads to scatter in the outer parts of the cluster. Therefore, the spread of temperature averaged over the whole cluster in the isothermal case increases with the cluster mass, while in the polytropic case, the scatter of temperature dominated by the core decreases with the cluster mass.

We found that the slopes of the mass-temperature relations obtained by us, both in the isothermal and polytropic cases, and for both spherical and triaxial halos, are similar to the those obtained in previous simulations and observations, while the proportionality coefficients are higher. The reason is partially due to the working definition of X-ray temperature or poor understanding of the evolutionary history of the intra-cluster gas.

Acknowledgements We are grateful to Prof. Feng Longlong for his guidance on this paper, and Prof. Jing Yipeng for helpful explanation regarding the statistical aspects of the triaxial dark matter halo model. This research is supported in part by the National Natural Science Foundation of China, and the National Key Basic Research Science Foundation of China.

References

- Afshordi N., Cen R., 2002, ApJ, 564, 669
 Bahcall N. A., Fan X., 1998, ApJ, 504, 1
 Balogh M. L., Babul A., Patton D. R., 1999, MNRAS, 307, 463
 Binney J., Tremaine S., 1987, Galactic Dynamics, Princeton: Princeton Univ. Press
 Birkinshaw M., Hughes J. P., Arnaud K. A., 1991, ApJ, 379, 466
 Blanchard A., Sadat R., Bartlett J. G., Le Dour M., 2000, A&A, 362, 809
 Blanton M., Cen R., Ostriker J. P., Strauss M. A., Tegmark M., 2000, ApJ, 531, 1
 Bond J. R., Myers S. T., 1996, ApJS, 103, 63
 Borgani S., Rosati P., Tozzi P., Stanford S. A., Eisenhardt P. R., Lidman C., Holden B., Della Ceca R., Norman C., Squires G., 2001, ApJ, 495, 80
 Byran G. L., Norman M. L., 1998, ApJ, 495, 80

- Bullock J. S., Kolatt T. S., Sigad Y., Somerville R. S., Kravtsov A. V., Klypin A. A., Primack J. R., Dekel A., 2001, MNRAS, 321, 559
- Buote D. A., Jeltema T. E., Canizares C. R., Garmire G. P., 2002, ApJ, 577, 183
- Eke V. R., Cole S., Frenk C. S., Patrick Henry J., 1998, MNRAS, 298, 1145
- Eke V. R., Cole S., Frenk C. S., 1996, MNRAS, 282, 263
- Eke V. R., Navarro J. F., Frenk C. S., 1998, ApJ, 503, 569
- Evrard A. E., Metzler C. A., Navarro J. F., 1996, ApJ, 469, 494
- Frenk C. S., et al., 1999, ApJ, 525, 554
- Henry J. P., 2000, ApJ, 534, 565
- Horner D. J., Mushotzky R. F., Scharf C. A., 1999, ApJ, 520, 78
- Inagaki Y., Sugimotohara T., Suto Y., 1995, PASJ, 47, 411
- Jing Y. P., Suto Y., 2002, ApJ, 574, 538 (JS02)
- Jing Y. P., Suto Y., 2000, ApJ, 529, L69
- Kitayama T., Suto Y., 1997, ApJ, 490, 557
- Komatsu E., Seljak U., 2001, MNRAS, 327, 1353
- Lewis G. F., Babul A., Katz N., Quinn T., Hernquist L., Weinberg D. H., 2000, ApJ, 536, 623
- Lee J., Suto Y., 2003, ApJ, 585, 151
- Makino N., Sasaki S., Suto Y., 1998, ApJ, 497, 555
- Mohr J. J., Evrard A. E., 1997, ApJ, 491, 38
- Moore B., Ghigna S., Governato F., Lake G., Quinn T., Stadel J., Tozzi P., 1999, ApJ, 524, 19
- Navarro J. F., Frenk C. S., White S. D. M., 1995, MNRAS, 275, 720
- Navarro J. F., Frenk C. S., White S. D. M., 1996, ApJ, 462, 563
- Navarro J. F., Frenk C. S., White S. D. M., 1997, ApJ, 490, 493
- Oguri M., Lee J., Suto Y., 2003, 599, 70
- Pearce F. R., Thomas P. A., Couchman H. M. P., Edge A. C., 2000, MNRAS, 317, 1029
- Peebles P.J.E. 1970, AJ, 75, 13
- Pen U., 1998, ApJ, 498, 60
- Pierpaoli E., Scott D., White M., 2001, MNRAS, 325, 77
- Seljak U., 2001, MNRAS, 325, 1359
- Suto Y., Sasaki S., Makino N., 1998, ApJ, 509, 544
- Viana P. T. P., Liddle A. R., 1996, MNRAS, 281, 323
- Viana P. T. P., Nichol R. C., Liddle A. R., 2002, ApJ, 569, 75
- Voit G. M., 2000, ApJ, 543, 113
- Wang L., Steinhardt P. J., 1998, ApJ, 508, 483
- White S. D. M., Efstathiou G., Frenk C. S., 1993, MNRAS, 262, 1023
- Xue Y. J., Wu X. P., 2000, A&A, 360, 43
- Yoshikawa K., Itoh M., Suto Y., 1998, PASJ, 50, 203
- Yoshikawa K., Jing Y. P., Suto Y., 2000, ApJ, 535, 593